Available online at www.sciencedirect.com
ScienceDirect
Mechanism and Machine Theory 43 (2008) 661–675
Mechanism and Machine Theory
www.elsevier.com/locate/mechmt

Capstan equation including bending rigidity and non-linear frictional behavior

Jae Ho Jung [a], Ning Pan [a,*], Tae Jin Kang [b]

[a] Division of Textile and Clothing, Department of Biological System Engineering, University of California, Davis, CA 95616, USA
[b] School of Materials Science and Engineering, Seoul National University, Seoul 151-742, South Korea

Received 20 March 2007; received in revised form 26 May 2007; accepted 9 June 2007
Available online 8 August 2007

Abstract

More rigorous analyses have been conducted in improving the classical capstan equation by including both the rod bending rigidity and a power-law friction (in place of the Amonton's law) into the formula. During the analyses, the power-law exponent was used as the indicator for the non-linear friction behavior, whereas both the capstan radius ratio and the incoming load incline angle were used as the parameters reflecting the bending rigidity. Our analyses indicate complex relationships those parameters have in influencing the tension ratio or tension transmitting efficiency, a thorough parametric study illustrates clearly such interconnections. Since in most cases, the bending rigidity of the tension member is non-negligible and non-linear friction is more common, the new results should be more useful in practical applications.

Keywords: Capstan equation; Bending rigidity; Non-linear friction; Radius ratio; Load incline angle; Apparent and actual tension ratios

1. Introduction

A tensioned rod, film, fiber or fabric in contact with a circular shaped body is frequently seen in many mechanical setups and applications. A well-known relationship governing the mechanism is the capstan equation [1], AKA Euler's equation of tension transmission:

$$T_1 = T_0 e^{\mu\theta} \tag{1a}$$

where T_1 and T_0 is the outgoing and incoming tensions, μ is the frictional coefficient between contacting solids, and θ is the contact angle. In pure mechanical viewpoint, a capstan is a typical free body under load equilibrium involving friction between rope or film-like tension member and a wheel like circular object. So the capstan equation is widely used to analyze the tension transmission behavior of a film/rope-like member in contact with a circular profiled surface such as in rope rescue system, marine cable application, computer storage device, clutch or brakes in vehicles, belt-pulley machine system, manufacturing of yarn, textile fabrics and fiber reinforced composites etc.

* Corresponding author.
E-mail address: npan@ucdavis.edu (N. Pan).

0094-114X/$ - see front matter © 2007 Elsevier Ltd. All rights reserved.
doi:10.1016/j.mechmachtheory.2007.06.002

However, many researchers have reported that the classical capstan equation Eq. (1a) does not hold for some cases, especially in textile processes. Two major problems have been identified. One is that the bending rigidity of the tension member, thus the radii of the two contacting objects into consideration has to be accounted for and a series of researches [2–5] were carried out to include the bending rigidity effect. The second improvement is to replace the over-simplified friction theory, the Amonton's law, with more advanced theories to better represent the polymer frictional behavior.

It has been generally accepted in polymer area that the frictional coefficient between fiber and other contacting surfaces is not a constant, altering with among other factors the initial tension. For example, Martin and Mittelmann [5] found that the frictional coefficient of the wool fiber measured by experiments, using the classical capstan equation, reduces by as much as 50% with the increase of the initial tension. Many studies [6,7,9–13] confirmed such friction drop and attempted to explain it. Yet most of them are based on empirical approaches in studying the effects of the initial tension, capstan radii and other parameters on the outgoing tension or the frictional coefficient. It has thus become clear that to understand this frictional drop in tension transmission, a reformulated basic relationship for fibrous materials between the frictional coefficient and the normal force is indispensable.

The first such attempt to adopt a non-linear relationship between frictional and normal forces in elucidating the frictional drop was made by Howell [10,11]. In the work, he improved the classical capstan equation by incorporating a power-law relationship between the frictional and normal forces, normalized by the radius of the contacting body. However, there are several remaining issues in Howell's approach. For instance, it is highly questionable of the properness to include the radius term in the frictional law, for friction should have nothing to do with the capstan radius. Also the tension member was considered as highly pliable so the bending rigidity was ignored, just as in the classical capstan equation. Moreover, his model has a critical defect that the calculated frictional coefficient could be greater than unity if increasing the radius of the contact body, which is against proven scientific evidence.

Therefore, the purpose of this research is to conduct a more rigorous analysis by taking both the bending rigidity of the tension member and a nonlinear friction law into consideration. No such analysis has been reported in public literature.

2. Theoretical approach

2.1. The modified Amonton's law of friction

Most widely accepted correction of the classical Amonton's law is the power-law between frictional and normal forces [8], the so called modified Amonton's law for textile materials looks as:

$$F_\mu = \alpha N^n, \quad n \leqslant 1 \tag{1b}$$

where F_μ and N are the frictional and normal forces, and n and α are appropriate material constants, respectively. Note that when $n = 1$, $\mu = \alpha$ so Eqs. (1a) and (1b) become identical and the power law reduces into the Amonton's law.

Eq. (1b) implies that the frictional coefficient μ depends on the normal force:

$$\mu = \frac{F_\mu}{N} = \frac{\alpha}{N^{1-n}} \tag{2}$$

Eq. (2) shows why this kind frictional behavior during tension transmission is often referred to as the friction drop because the frictional coefficient decreases with the increases of the normal force.

2.2. Equilibrium equations in contact region

Fig. 1 shows the free body diagram of a rod wound over a circularly shaped body (the capstan). From the force balances along 1 and 2 directions and moment equilibrium at point "O", the following three equations, termed the classical capstan equation, can be derived.

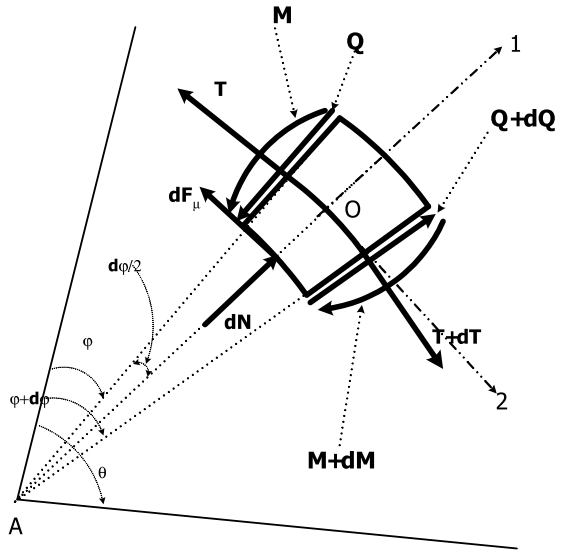

Fig. 1. Free body diagram of a rod in contact with a circularly shaped body.

$$\mathrm{d}T + Q\mathrm{d}\varphi - \mathrm{d}F_\mu = 0 \tag{3}$$

$$\mathrm{d}Q - T\mathrm{d}\varphi + \mathrm{d}N = 0 \tag{4}$$

$$\mathrm{d}M - QR\mathrm{d}\varphi + r_1\mathrm{d}F_\mu = 0 \tag{5}$$

$$\rho = r_2/r_1, \quad R = r_1 + r_2$$

where T, Q, M are the tension, shear force and bending moment, respectively; φ is an angle measured from the start point of contact to a given point in the contact region; θ the complete contact angle, r_1 and r_2 are the corresponding radius of the rod and the contact body. Also, all the existent contacts are regarded as continuous.

2.3. Solutions for the capstan equation with power law friction

For comparison, the classical capstan equation combined with the power friction law is given below by setting $Q = M = r_1 = 0$. The resultant equations read:

$$\mathrm{d}T - \mathrm{d}F_\mu = 0 \tag{6}$$

$$\mathrm{d}N = T\mathrm{d}\varphi \tag{7}$$

Combining Eqs. (6) and (7) with Eq. (1) gives:

$$\frac{\mathrm{d}N}{\mathrm{d}\varphi} = \alpha N^n, \quad T = \alpha N^n \tag{8}$$

The solutions of Eq. (8) are given as:

$$N^{1-n} - \{N(0)\}^{1-n} = \alpha(1-n)\varphi \tag{9}$$

$$T(\varphi) = \alpha\left[\alpha(1-n)\varphi + \left\{\frac{T(0)}{\alpha}\right\}^{\frac{1-n}{n}}\right]^{\frac{n}{1-n}} \tag{10}$$

So the outgoing tension T_2 is expressed as:

$$T_2 = \alpha\left[\alpha(1-n)\theta + \left\{\frac{T_1}{\alpha}\right\}^{\frac{1-n}{n}}\right]^{\frac{n}{1-n}} \tag{11}$$

Eq. (11) is the capstan equation with the power friction law, yet ignoring the effect of the rod bending rigidity. It shows that the tension transmission ratio or tension ratio T_2/T_1 is not constant at given value of q with different choice of T_1. Thus the frictional coefficient $\mu = 1/\theta \cdot \ln(T_2/T_1)$ defined in Martin and Mittelmann's paper [5] would yield different results when using our result of Eq. (11), as:

$$\mu = \frac{1}{\theta}\ln\frac{T_2}{T_1} = \frac{1}{\theta}\left[\frac{n}{1-n}\ln\left\{\alpha(1-n)\theta + \left(\frac{T_1}{\alpha}\right)^{\frac{1-n}{n}}\right\} + \ln\alpha - \ln T_1\right] \tag{12}$$

and adopting Howell's results in Refs. [10] and [11] leads to:

$$\mu = \frac{1}{\theta}\ln\frac{T_2}{T_1} = \frac{\ln\left[1 + \alpha(1-n)\left(\frac{r_2}{T_1}\right)^{1-n}\theta\right]}{\theta(1-n)} \tag{13}$$

One can easily find out that both Eqs. (12) and (13) show a decreasing tendency of frictional coefficient with the increase of the initial tension T_1. However, the most critical flaw of Eq. (13), as mentioned above, is that the value of the frictional coefficient also depends on the radius of the capstan r_2 and can be greater than unity when r_2 is high enough, at given values of α, n, θ and T_1. This problem stems from the frictional law used in Howell's approach [10,11]:

$$\frac{1}{R}\frac{\mathrm{d}F_\mu}{\mathrm{d}\varphi} = \alpha\left(\frac{1}{R}\frac{\mathrm{d}F_\mu}{\mathrm{d}\varphi}\right)^n \tag{14}$$

2.4. Solutions when including the rod bending rigidity

To include its bending rigidity, the rod is considered as a linear elastic material so the bending constitutive equations are:

$$M = \frac{EI}{R} = \frac{E}{R}\cdot\frac{\pi r_1^4}{4}, \quad \mathrm{d}M = 0 \tag{15}$$

Rearranging Eqs. (3)–(5) by using Eqs. (1) and (5) and then integrating the results give:

$$\frac{\mathrm{d}^2T}{\mathrm{d}\varphi^2} + \frac{\rho}{n}\left(\frac{1+\rho}{\alpha\rho}\right)^{\frac{1}{n}} T^{\frac{1-n}{n}}\cdot\frac{\mathrm{d}T}{\mathrm{d}\varphi} - \rho T = 0 \tag{16}$$

$$Q = \frac{1}{\rho}\cdot\frac{\mathrm{d}T}{\mathrm{d}\varphi}, \quad \mathrm{d}F_\mu = \frac{1+\rho}{\rho}\mathrm{d}T, \quad \mathrm{d}N = \frac{1}{n}\left(\frac{1+\rho}{\alpha\rho}\right)^{\frac{1}{n}}\cdot T^{\frac{1-n}{n}}\mathrm{d}T, \quad M = \frac{EI}{R} \tag{17}$$

Eq. (16) together with Eq. (17) is the new governing equation of the model, accounting for both rod bending rigidity and power law friction. It is interesting to note that the modulus E of the rod is not involved in Eq. (16), i.e., the calculated tension ratio will be independent of the rod modulus. In fact the modulus E only influences the equilibrium configuration of the rod in the non-contact region, and thus the individual value of incoming and outgoing tensions (see Refs. [3,4] for more details). Generally speaking, the rod bending rigidity depends on its radius and modulus E. Whereas to the tension ratio, only the rod radius ratio $\rho = r_2/r_1$ is relevant, where the capstan radius r_2 remains a constant. Thus the radius ratio ρ can be regarded as the parameter reflecting the bending rigidity effect on the tension ratio. The solution of Eq. (16) yields the desired new capstan equation including both the bending rigidity and the power law friction.

2.5. Boundary conditions

To find boundary conditions, let us consider the bent rod in contact with circular body as show in the following Fig. 2. Apparently, the inclined angles ω_1 and ω_2 will be zero in case of no rigidity. On the other hand, these angles become indispensable for a rod with bending rigidity to make an equilibrium shape (see more in Ref. [3]). From Fig. 2, we have the following relationships:

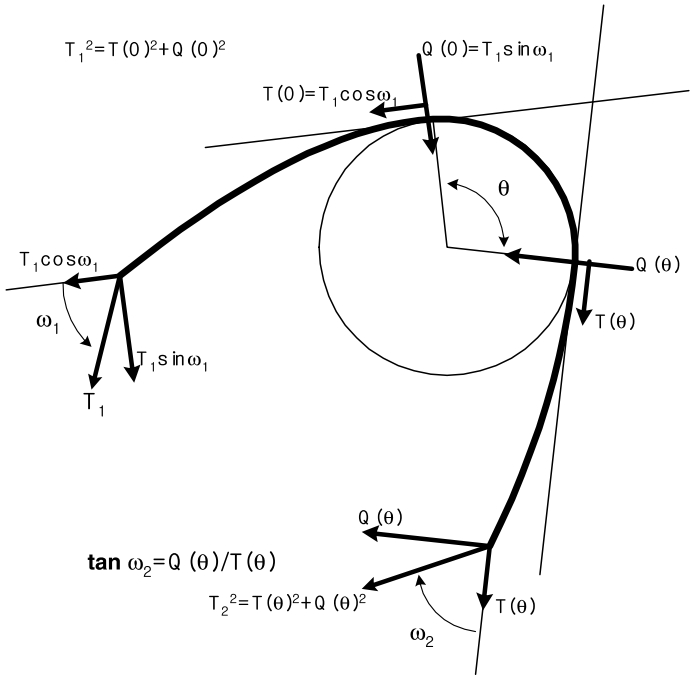

Fig. 2. Whole view of bent rod in contact with circular body.

$$T(0) = T_1 \cos\omega_1, \quad Q(0) = \frac{T'(0)}{\rho} = T_1 \sin\omega_1, \quad T_1 = \sqrt{\{T(0)\}^2 + \{Q(0)\}^2} \tag{18}$$

$$T_2 = \sqrt{\{T(\theta)\}^2 + \{Q(\theta)\}^2}, \quad \tan\omega_2 = \frac{Q(\theta)}{T(\theta)} = \frac{T'(\theta)}{\rho T(\theta)} \tag{19}$$

2.6. Expression of the tension ratio

In Eqs. (18) and (19) it is clear that the inclined angles (ω_1, ω_2) of the load affect the direction of incoming and outgoing tensions T_1 and T_2. Apart from this, there exists an essential difference between the expression of $T(\theta)$ in and without the rod rigidity. To distinguish the two cases, we define two corresponding tension ratios – an apparent tension ratio τ_A, and an actual tension ratio τ_C, respectively as:

$$\tau_A = \sqrt{\frac{\{T(\theta)\}^2 + \{Q(\theta)\}^2}{\{T(0)\}^2 + \{Q(0)\}^2}} = \sqrt{\frac{\rho^2\{T(\theta)\}^2 + \{T'(\theta)\}^2}{\rho^2\{T(0)\}^2 + \{T'(0)\}^2}}, \tag{20a}$$

and

$$\tau_C = \frac{T(\theta)}{T(0)} \tag{20b}$$

where the prime indicates the differentiation with respect to θ.

Eq. (20) shows the difference in the expression between tension ratios with and without the rod rigidity. If the value of ω_1 and ω_2 become zero, τ_A will be the same as τ_C. Thus we can compare the two tension ratios τ_C and τ_A to investigate the effect of the inclined angle on the tension ratio, and compare τ_C with the classical capstan Eq. (11) to examine the influence of the rod bending rigidity.

2.7. Capstan equation with rod rigidity and the Amonton's friction law

If we set $n = 1$ Eq. (2) so that $\alpha = \mu$, Eq. (16) simplifies into one with Amonton's law:

$$\mu\frac{d^2T}{d\varphi^2} + (1+\rho)\cdot\frac{dT}{d\varphi} - \mu\rho T = 0 \tag{21}$$

Applying Eq. (18) in solving the above differential equation gives the following solution:

$$T(\theta) = D_1 e^{-a\theta} + D_2 e^{b\theta} \tag{22a}$$

$$D_1 = \frac{T_1(b\cos\omega_1 - \rho\sin\omega_1)}{a+b}, \quad D_2 = \frac{T_1(a\cos\omega_1 + \rho\sin\omega_1)}{a+b} \tag{22b}$$

$$a = \frac{1+\rho+\sqrt{(1+\mu)^2+4\mu^2\rho}}{2\mu}, \quad b = \frac{-1-\rho+\sqrt{(1+\rho)^2+4\mu^2\rho}}{2\mu} \tag{22c}$$

Substituting the above results into Eq. (20) gives the following:

$$\tau_A = \sqrt{\frac{D_1^2(1+\frac{a^2}{\rho^2})e^{-2a\theta} + 2D_1D_2(1-\frac{ab}{\rho^2})e^{-a\theta}e^{b\theta} + D_2^2(1+\frac{b^2}{\rho^2})e^{2b\theta}}{D_1^2(1+\frac{a^2}{\rho^2}) + 2D_1D_2(1-\frac{ab}{\rho^2}) + D_2^2(1+\frac{b^2}{\rho^2})}} \tag{23a}$$

and

$$\tau_C = \frac{D_1 e^{-a\theta} + D_2 e^{b\theta}}{D_1 + D_2} \tag{23b}$$

Eq. (23a) is the capstan equation with rigidity, including the effect of the inclined angles of tension, whereas Eq. (23b) provides the actual tension ratio at the contact points. Both are newly derived in the present analysis, and their behaviors will be studied by parametric analysis in a later section.

2.8. Capstan equation with rod rigidity and power-law friction

Since we cannot get an analytical solution for Eq. (16), numerical procedure is required. Using the 4th order Runge–Kutta method, we can calculate the tension $T(\varphi)$ with the boundary conditions from Eq. (18):

$$T'(\varphi) = U(\varphi) \tag{24}$$

$$U'(\varphi) = -\frac{\rho}{n}\left(\frac{1+\rho}{\alpha\rho}\right)^{\frac{1}{n}}\{T(\varphi)\}^{\frac{1-n}{n}}U(\varphi) + \rho T(\varphi) \tag{25}$$

$$T(0) = T_1\cos\omega_1, \quad U(0) = \rho T_1\sin\omega_1 \tag{26}$$

where the prime indicates the differentiation to φ. Once the solution is obtained numerically, the values of τ_A and τ_C can be calculated. Selected examples will be dealt with in next session.

3. Results and discussions

3.1. Tension ratio in case of no inclined angle

To investigate the effect of radius ratio and power-law friction under no influence of inclined angle of load, let us consider the following examples. The other major parameters are chosen as $0° \leqslant \theta \leqslant 180°$, $n = 0.67$ and $\omega_1 = 0°$.

Example 1: $\rho = 5,\ \alpha = 0.4,\ T_1 = 1$
Example 2: $\rho = 5,\ \alpha = 0.6,\ T_1 = 1$
Example 3: $\rho = 100,\ \alpha = 0.4,\ T_1 = 1$
Example 4: $\rho = 5,\ \alpha = 0.4,\ T_1 = 0.1$

where the first example serves as a reference showing the effect of radius ratio and power-law friction on the tension ratio. The second example show the effect of increased frictional coefficient, third the increased radius ratio (rod bending rigidity), and fourth the initial tension respectively. Of course, even if we put the inclined angle ω_1 as zero, the apparent tension ratio τ_A is slightly different from the actual tension ratio τ_C due to the

existence of rod rigidity (associated shear force). However, its difference is negligible in the above examples. So we use the apparent tension ratio τ_A for calculation.

Figs. 3–6 show the comparison of the tension ratios from the above examples with the data for the case of classical capstan equation (no rod rigidity) with power-law friction. In Figs. 3–5 it is clear that by adopting the power-law friction, the outgoing tensions are greatly decreased compared with the data without this modification. (the solid lines versus the dotted one of the same color). In Fig. 3, the decrease of the tension ratio is by 54.1% in case of no rigidity, and 47.3% in case of with rigidity ($\rho = 5$), both at almost half the initial tension values. Fig. 4 shows the data with higher frictional coefficient $\alpha = 0.6$. It shows the same tendency as that in Fig. 3, but with further reduction in tension ratio, 66.2% in case of no rigidity, 57.1% in case of $\rho = 5$. So it can be inferred that the increase of frictional coefficient enhances the tension ratio decrease due to power-law friction.

Conversely, the radius ratio, or the rod bending rigidity compensates such friction caused decreases, albeit slightly – from 54.1% to 47.3% and from 66.2% to 57.1%, with and without the rod bending rigidity, respectively. We call this feature as the first coupling effect of rod rigidity on the reduction of the tension ratio due to power-law friction. Also this coupling effect is enhanced with the increase of the frictional coefficient.

Meanwhile, we can confirm the influence of the rod rigidity on such tension ratio reduction at different frictional behaviors from the Figs. 3 and 4. (Compare the two dotted, or solid, line with each other.) In Figs. 3 and 4 it is 21.8% and 33.8% for Amonton's friction, 22.9% and 34.9% for power-law friction respectively. So the reverse coupling effect, from 21.8% to 22.9% and from 33.8% to 34.9% with and without the bending rigidity, slightly higher tension ratio reduction due to the existence of rod rigidity.

However, if the radius ratio jumps from 5 to 100, the effect of rod rigidity virtually disappeared as seen in Fig. 5. The huge tension ratio drop due to adopting power-law friction still exists. Unlike other figures, the Fig. 6 shows distinct tendency. It is remarkable that the tension ratio with the power-law friction does not

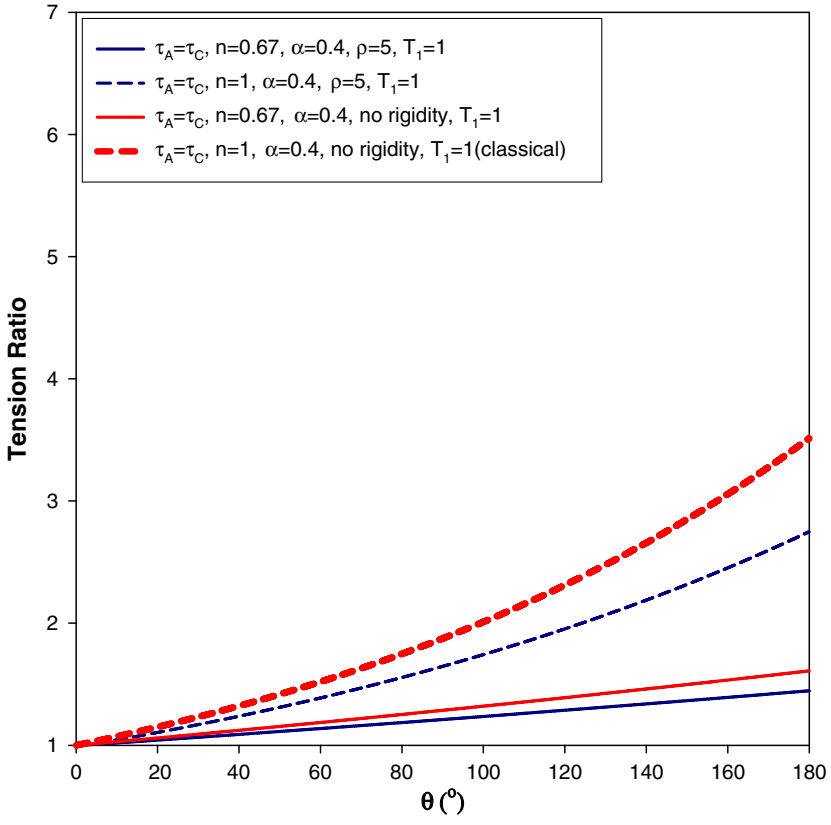

Fig. 3. Comparison of the tension ratios in case of $\alpha = 0.4$, $n = 0.67$, 1, $T_1 = 1$, $\rho = 5$ and $\omega = 0°$.

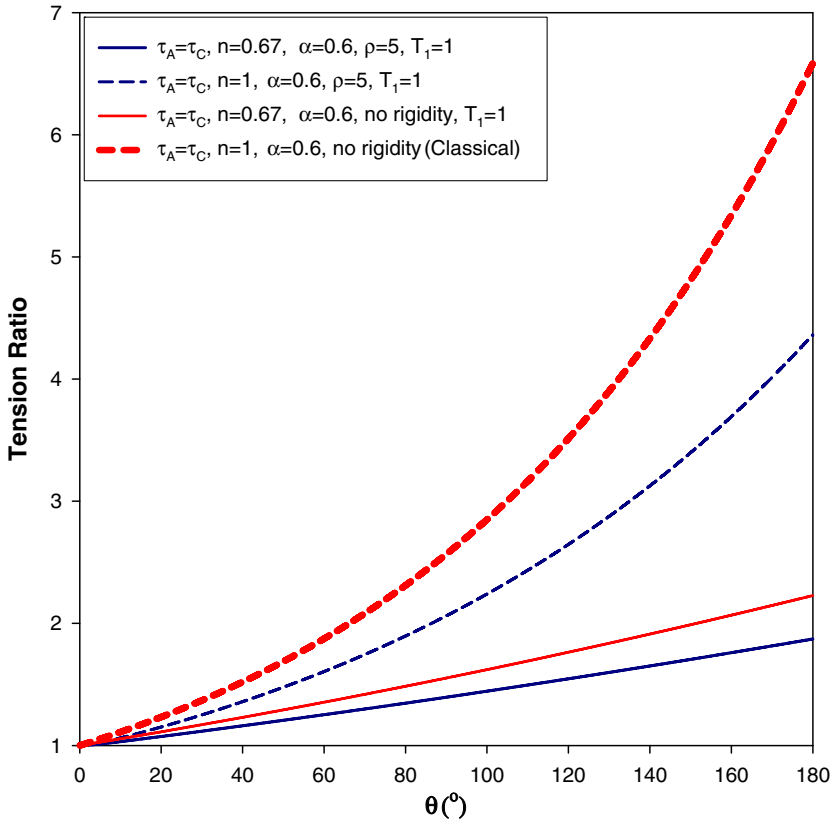

Fig. 4. Comparison of the tension ratios in case of $\alpha = 0.6$, $n = 0.67$, 1, $T_1 = 1$, $\rho = 5$ and $\omega = 0°$.

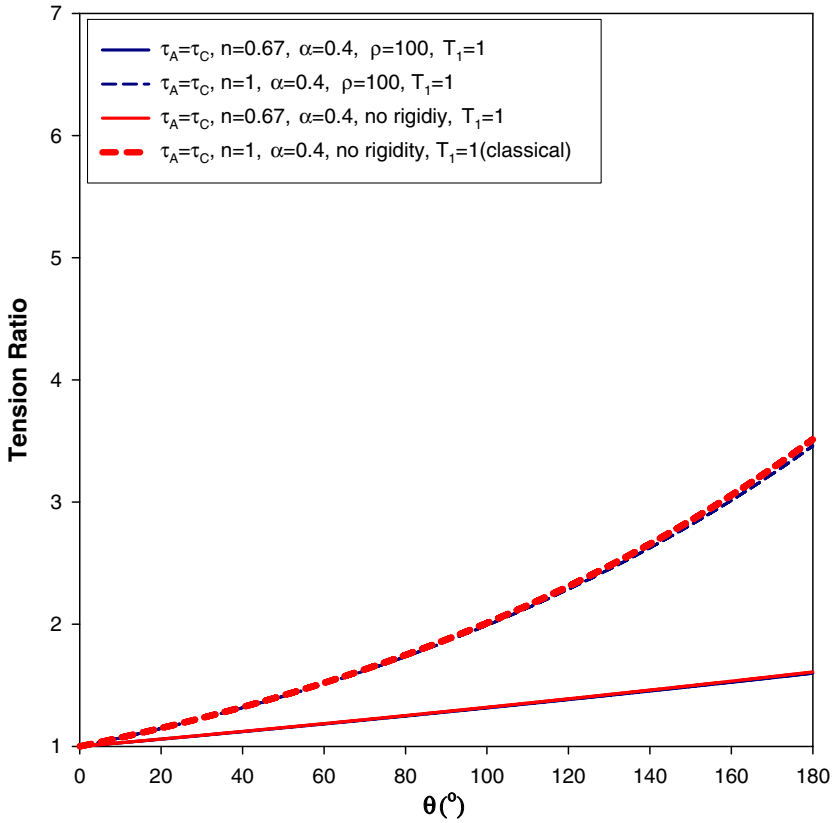

Fig. 5. Comparison of the tension ratios in case of $\alpha = 0.4$, $n = 0.67$, 1, $T_1 = 1$, $\rho = 100$ and $\omega = 0°$.

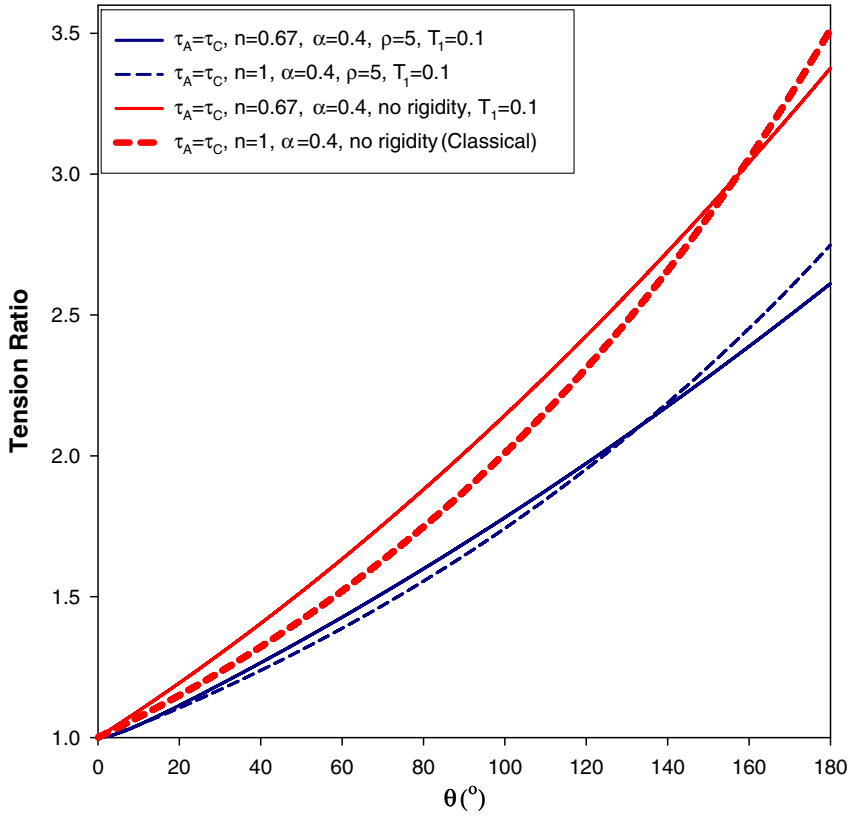

Fig. 6. Comparison of the tension ratios in case of $\alpha = 0.4$, $n = 0.67$, 1, $T_1 = 0.1$, $\rho = 5$ and $\omega = 0°$.

always reaches higher value than the tension ratio with the Amonton's law, while the decrease of the tension ratio due to rod bending rigidity persists.

Fig. 7 shows the calculated data of the apparent tension ratio τ_A in case of different incoming tension levels $T_1 = 0.1$, 0.5, 1, 5, 10. It is also remarkable that the tension ratio heavily depends on the initial tension. Neither the classical capstan equation nor the capstan equation with rigidity only shows such tendency, i.e., the power-law seems to be responsible. In both classical capstan Eq. (1a) and classical capstan including the bending rigidity in Eq. (22), the tension ratio $T(\theta)/T_1$ can be expressed explicitly in terms of other parameters. However, such normalization is not possible in the classical capstan including the power law friction in Eq. (11). Similarly, the numerical solution from the Eq. (16) shows such characteristics as well. This stems from the mathematical feature of Eq. (8), and this non-linear feature of frictional law prohibits normalizing Eqs. (10) and (16) with the initial tension T_1. It also renders the frictional coefficient calculated in Eq. (12) to decrease with the initial tension T_1 as observed in Martin and Mittelmann's data (see Fig. 6 in Ref. [5]).

So in Fig. 7 a smaller initial tension results in a larger tension ratio. Now we can conclude that there are two parameters in determining the tension ratio in a coupled way: the power law friction has to be used so that the tension ratio will be lower than predicted by the classic capstan equation on one hand, and the tension ratio also becomes dependent on the initial tension, and increases as the initial tension decreases. In other words, the initial tension has to be sufficiently large to see a reduction in tension ratio caused by the power-law friction. This explains why we don't see the drop in tension ratio in Fig. 6 even after the power-law friction is adopted; the initial tension $T_1 = 0.1$ is just too smaller for such a drop to be visible.

In summary, both power-law friction and rod rigidity decreases the tension ratio. Smaller value of radius ratio, power-law exponent, and larger value of initial tension results in the decrease of tension ratio. More dominant factor is power-law friction, but the initial tension should be sufficiently large. In addition, there exist coupling effects between the power-law friction and the bending rigidity of the rod.

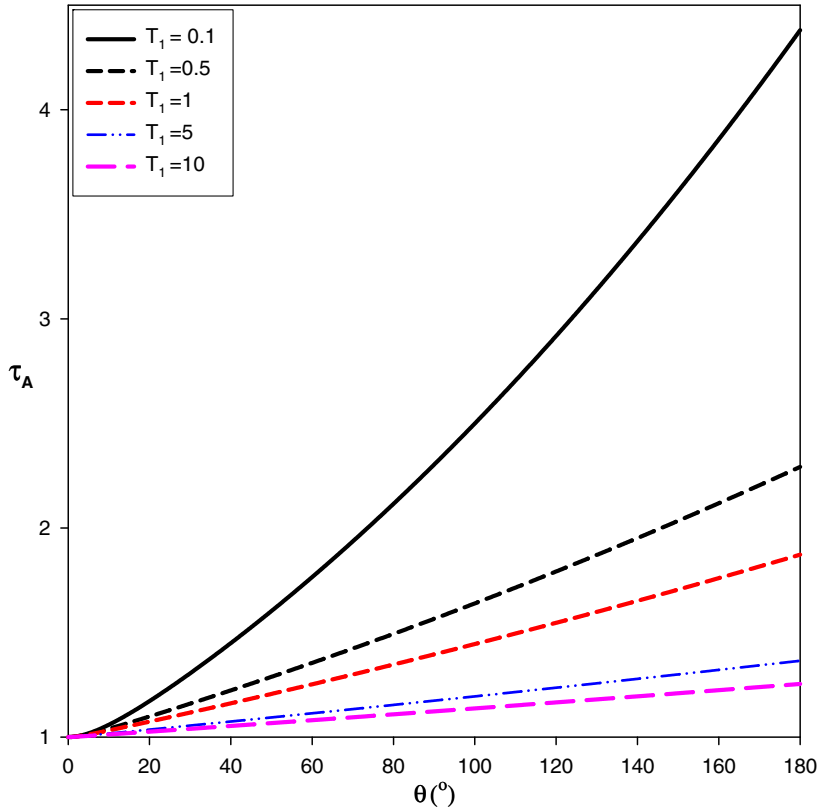

Fig. 7. Comparison of the apparent tension ratios in case of $T_1 = 0.1, 0.5, 1, 5, 10$.

3.2. Tension ratio in the existence of inclined angle

Next, we consider the influence of the non-zero inclined angle of load $\omega_1 = 40°$ on the examples below, with $n = 0.67$:

Example 5: $\rho = 5,\ \alpha = 0.4,\ T_1 = 1$
Example 6: $\rho = 5,\ \alpha = 0.6,\ T_1 = 1$
Example 7: $\rho = 100,\ \alpha = 0.4,\ T_1 = 1$
Example 8: $\rho = 5,\ \alpha = 0.4,\ T_1 = 0.1$

Since the inclined angle $\omega_1 \neq 0°$, the apparent and actual tension ratio becomes different from each other. Figs. 8–11 show the apparent and actual tension ratios according to the above examples compared with the classical capstan equation ($n = 1$), and power-law friction with no rigidity. The general tendency is that the apparent tension ratio τ_A is always smaller than the actual tension ratio τ_C. it is also interesting that the apparent tension ratio may be smaller than unity at a certain range of contact angle, while the actual ratio always exceeds 1. So it can be inferred that the existence of shear force decreases the tension ratio. Another expected feature is that τ_A is also smaller than the tension ratio from the classical capstan equation. But this tendency does not hold true for τ_C. In Figs. 8, 10 and 11, τ_C is almost greater than the tension ratio from the classical capstan equation. Only Fig. 9 shows that the tension ratio from the classical capstan equation may be greater than τ_C, but it is not clear whether this is entirely due to the inclined load angle ω_1.

To further clarify it, Fig. 12 is presented which shows the actual tension ratio τ_C in case of $\alpha = 0.4$, $n = 0.67$, $T_1 = 0.1$, $\rho = 5$ with different choices of $\omega_1 = 0°, 20°, 40°, 60°$. In the previous examples, we recognized that the power-law friction and rod rigidity decrease the tension ratio. However, it is also clear from the Fig. 12 that the inclined angle enhances the tension ratio. So the net effect shows up as the result of competition of

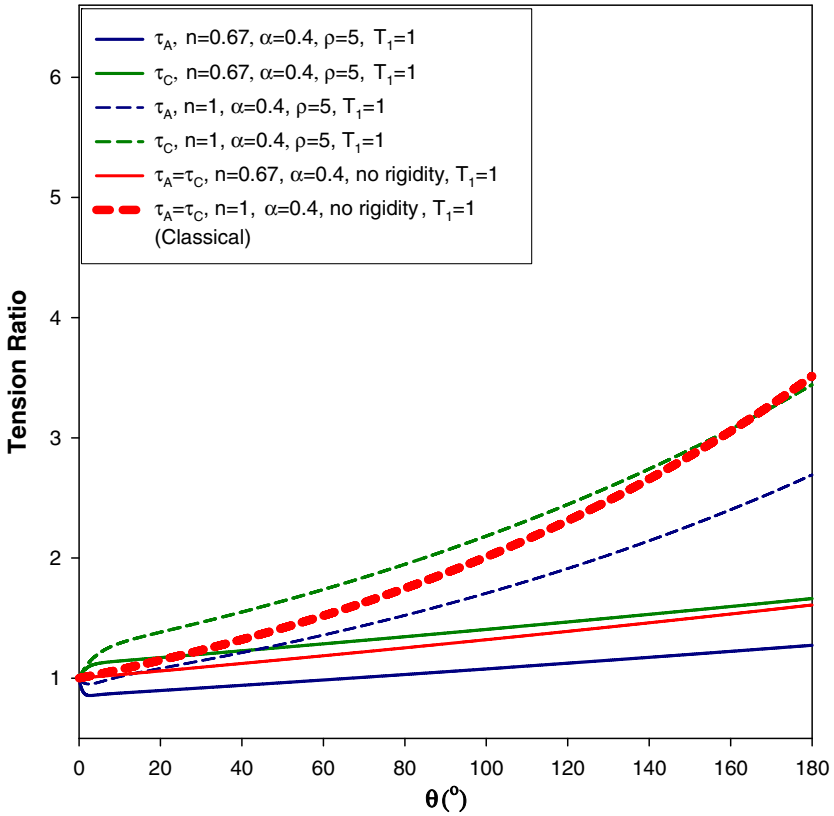

Fig. 8. Comparison of the tension ratios in case of $\alpha = 0.4$, $n = 0.67$, 1, $T_1 = 1$, $\rho = 5$ and $\omega = 40°$.

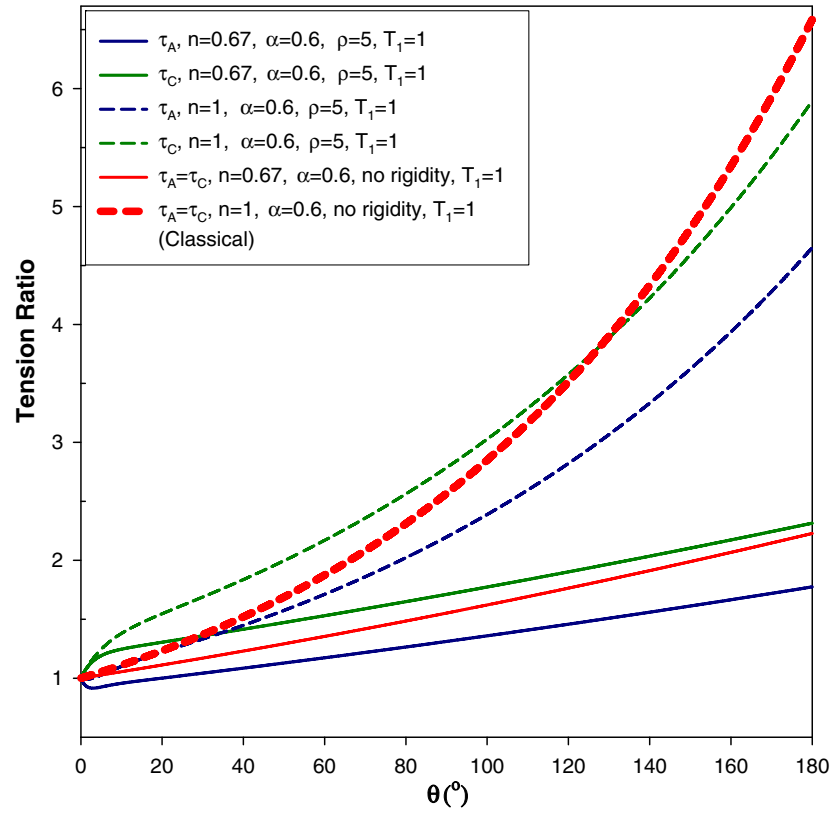

Fig. 9. Comparison of the tension ratios in case of $\alpha = 0.6$, $n = 0.67$, 1, $T_1 = 1$, $\rho = 5$ and $\omega = 40°$.

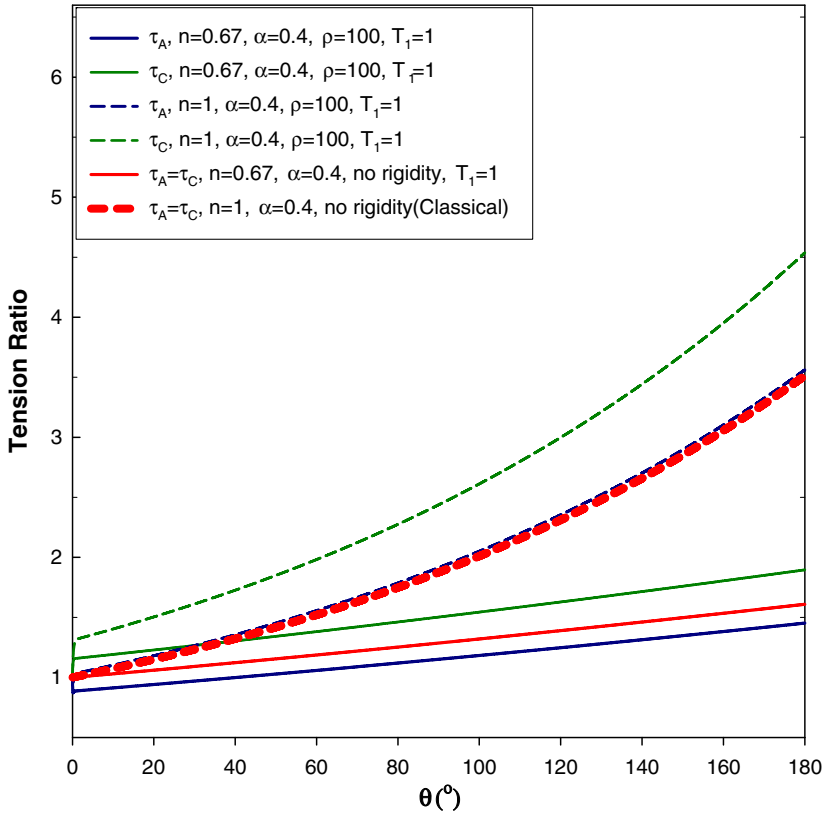

Fig. 10. Comparison of the tension ratios in case of $\alpha = 0.4$, $n = 0.67$, 1, $T_1 = 1$, $\rho = 100$ and $\omega = 40°$.

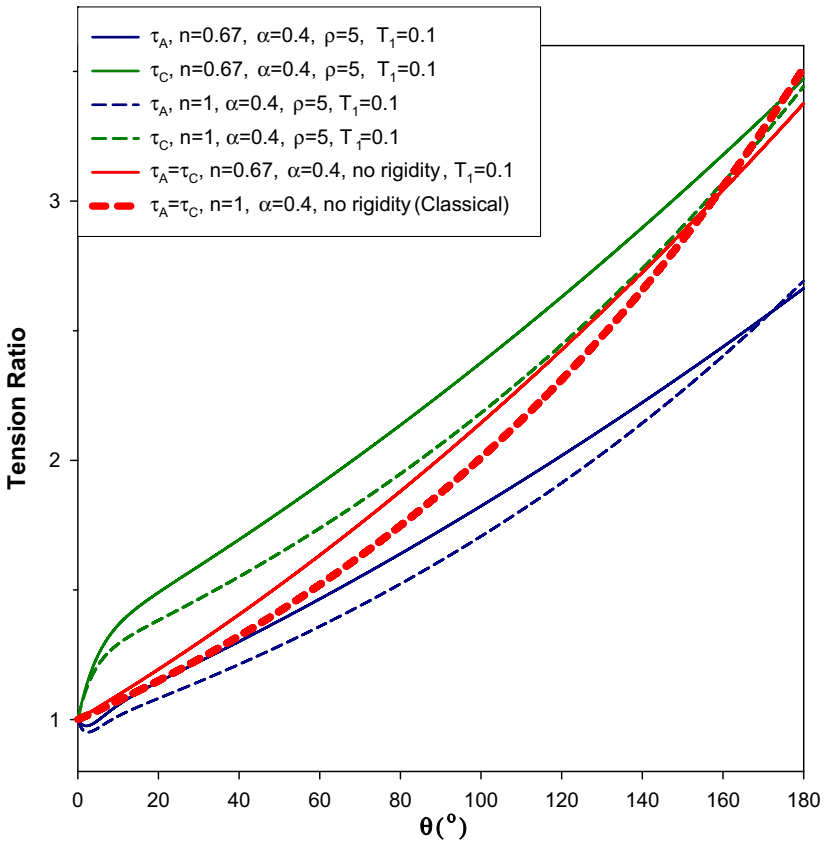

Fig. 11. Comparison of the tension ratios in case of $\alpha = 0.4$, $n = 0.67$, 1, $T_1 = 0.1$, $\rho = 100$ and $\omega = 40°$.

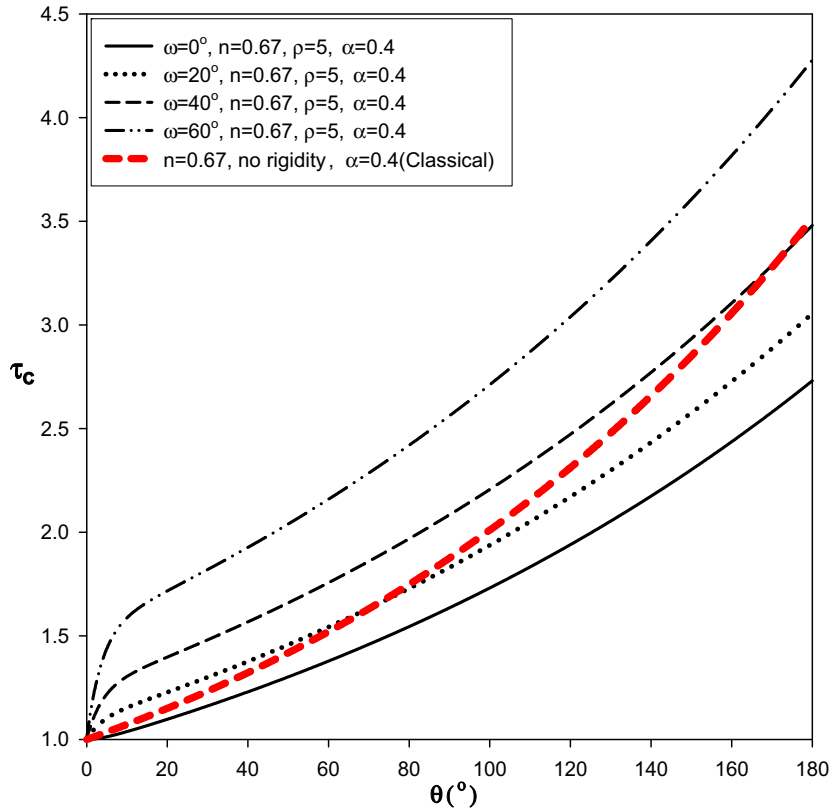

Fig. 12. Actual tension ratio τ_C in case of $\alpha = 0.4$, $n = 0.67$, $T_1 = 0.1$, $\rho = 5$ with different choices of $\omega = 0°$, 20°, 40°, 60°.

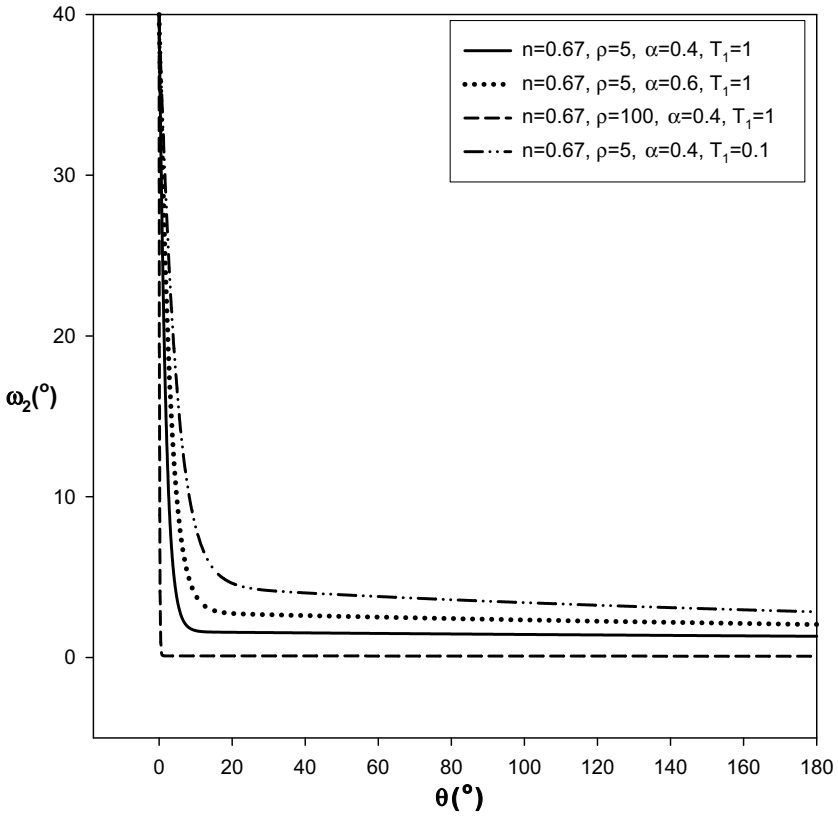

Fig. 13. Inclined angle of load ω_2 versus contact angle θ in the example 5, 6, 7 and 8.

these factors. Another interesting feature is that only the tension ratios using power-law friction (solid lines) are greater than those using the Amonton's law in Fig. 11. This again is due to the low initial tension T_1, so the tension ratio drop caused by the power-law friction is not visible. In addition, the influence on the inclined angle of load for the outgoing tension ω_2 by the contact angle θ is shown in Fig. 13.

It shows that the inclined angle ω_2 drops abruptly from 40° and reaches a certain limit point within the range of $0° < \omega_2 < 10°$ as the contact angle grows larger. However, it only become zero in case of $\rho = 100$ when the bending rigidity effect is small, for large rod rigidity prohibits ω_2 from being zero. Of course, different choices of ω_1 render different ranges of ω_2 as well.

4. Conclusions

More rigorous analyses have been conducted in this paper to improve the classical capstan equation by including both the bending rigidity and the frictional drop effects. A thorough parametric analysis has been carried out and the following conclusions are drawn.

1. Either using the power-law friction, or including the rod bending rigidity changes the tension ratio. A smaller radius ratio ρ, or a smaller power-law exponent α can result in the decrease of tension ratio. However such influences become visible only when the initial tension T_1 is sufficiently large. In terms of impact on the tension ratio, the power-law friction is more significant than rod bending rigidity, but there exist coupling effects between the two as well.
2. The effect of bending rigidity on the tension ratio can be reflected by two parameters – the radius ratio ρ and inclined angle of load ω_1. Calculated tension ratios without rod bending rigidity are always greater than those with rigidity. The existence of inclined angle of load ω_1 makes the apparent tension ratio between incoming and outgoing tension different from the actual tension ratio between the values of start and end point of contact. It is also interesting that the apparent tension ratio may be smaller than unity at a certain range of contact angle, while the actual ratio always exceeds 1.
3. A greater inclined angle ω_1 enhances the tension ratio, thus competing with the effects of power-law friction and rod rigidity. Furthermore, the existence of rod rigidity prohibits the inclined load angle for outgoing tension ω_2 from being zero but suppresses it rapidly to a small value. Overall, by including the effects of both rod bending rigidity and the power law friction during tension transmission, the new model is more robust, able to provide more realistic and accurate predictions.

Acknowledgements

This work was supported by the Korea Research Foundation Grant funded by the Korean Government (MOEHRD, KRF-2005-214-D000407), and National Textile Center (NTC) in University of California at Davis.

References

[1] W.E. Morton, J.W.S. Hearle, Physical Properties of Textile Fibres, second ed., Heinemann, London, 1975, pp. 611.
[2] J.M. Stuart, Capstan equation for strings with rigidity, Brit. J. Appl. Phys. 12 (1961) 559–562.
[3] Jae Ho Jung, Tae Jin Kang, Jae Ryoun Youn, Effect of bending rigidity on the capstan equation, Text. Res. J. 74 (12) (2004) 1085–1096.
[4] Jae Ho Jung, Ning Pan, Tae Jin Kang, Tension transmission via an elastic rod gripped by two circular edged plates, Int. J. Mech. Sci., in press.
[5] A.J.P. Martin, R. Mittelmann, Some measurements of the friction of wool and mohair, J. Text. Inst. (1946) T269–T280.
[6] M.E. Baird, Mieszkis, Friction properties of nylon yarn and their relations to the function of textile guide, J. Text. Inst. 46 (6) (1955) T101.
[7] J.O. Ajayi, H.M. Elder, Effect of surface geometry on fabric friction, J. Test. Eval. 25 (1997) 182.
[8] F.P. Bowden, J.E. Young, Friction of diamond, graphite, and carbon and the influence of surface films, Proc. Roy. Soc. A208 44 (1951) 444.

[9] J.O. Ajayi, H.M. Elder, Comparative studies of yarn and fabric friction, J. Test. Eval. 22 (1994) 463.
[10] H.G. Howell, The general case of friction of a string round a cylinder, J. Text. Inst. 44 (8) (1953) T359–T362.
[11] H.G. Howell, The friction of a fiber round a cylinder and its dependence upon cylinder radius, J. Text. Inst. 45 (8) (1954) T359–T362.
[12] J.S. Olsen, Friction behavior of textile yarns, Text. Res. J. 39 (1969) 31.
[13] Jun Lang Sukang Zhu, Ning Pan, Frictional behavior of synthetic yarns during processing, Text. Res. J. 73 (2004) 227–231.